




Combining Hough Transform and Fuzzy Unsupervised Learning Strategy in Automatic Segmentation of Large Bowel Obstruction Area from Erect Abdominal Radiographs

Kwang Baek Kim^{1*} , Doo Heon Song², and Hyun Jun Park³, *Member, KIICE*

¹Department of Artificial Intelligence, Silla University, Busan 46958, Republic of Korea

²Department of Computer Games, Yong-in Art & Science University, Yongin 17145, Republic of Korea

³Department of Artificial Intelligence Software, Cheongju University, Cheongju 28503, Republic of Korea

Abstract

The number of senior citizens with large bowel obstruction is steadily growing in Korea. Plain radiography was used to examine the severity and treatment of this phenomenon. To avoid examiner subjectivity in radiography readings, we propose an automatic segmentation method to identify fluid-filled areas indicative of large bowel obstruction. Our proposed method applies the Hough transform to locate suspicious areas successfully and applies the possibilistic fuzzy c-means unsupervised learning algorithm to form the target area in a noisy environment. In an experiment with 104 real-world large-bowel obstruction radiographs, the proposed method successfully identified all suspicious areas in 73 of 104 input images and partially identified the target area in another 21 images. Additionally, the proposed method shows a true-positive rate of over 91% and false-positive rate of less than 3% for pixel-level area formation. These performance evaluation statistics are significantly better than those of the possibilistic c-means and fuzzy c-means-based strategies; thus, this hybrid strategy of automatic segmentation of large bowel suspicious areas is successful and might be feasible for real-world use.

Index Terms: Erect Radiography, Hough Transform, Large Bowel Obstruction, Possibilistic FCM

I. INTRODUCTION

Bowel obstruction or intestinal obstruction refers to the partial or complete blockage of the small or large bowel, which prevents normal movement as a result of digestion. Unlike paralytic ileus that involves a functional motor paralysis of the digestive tract, mechanical bowel obstruction occurs due to adhesions, compression, torsion, or overlap, and generally requires operational treatment. Thus, it is important to decide the appropriate time and level of the treatment [1]. The signs and symptoms of bowel obstruction include squeezing abdominal pain, vomiting, bloating, nau-

sea, abdominal distension, and constipation [1,2]. In Korea, approximately 68,000 patients with intestinal obstruction were reported in 2022, half of which over 60 years old; the resulting medical expense was over 66 million US dollars [3]. As per a US report, bowel obstruction was responsible for 15% of hospital admissions with acute abdominal pain, and several cases required acute surgical care [4].

Large bowel obstruction (LBO) differs substantially from small bowel obstruction (SBO) in several aspects. LBO accounts for 20% of all mechanical obstructions. Its etiology is age-dependent, with colorectal cancer being the most common cause in adults [5-7]. Although LBO may develop over


Received 22 September 2023, Revised 23 October 2023, Accepted 25 October 2023

*Corresponding Author Kwang Baek Kim (E-mail: gbkim@silla.ac.kr)

Department of Artificial Intelligence, Silla University, Busan 46958, Republic of Korea

Open Access <https://doi.org/10.56977/jicce.2023.21.4.322>

print ISSN: 2234-8255 online ISSN: 2234-8883

 This is an Open Access article distributed under the terms of the Creative Commons Attribution Non-Commercial License (<http://creativecommons.org/licenses/by-nc/3.0/>) which permits unrestricted non-commercial use, distribution, and reproduction in any medium, provided the original work is properly cited.

Copyright © The Korea Institute of Information and Communication Engineering

a protracted period, its clinical presentation is often acute [8]. If left untreated, blockage cuts off the blood supply to the colon, causing partial necrosis that can result in high morbidity and fatality rates [9].

Abdominal radiography is generally the initial diagnostic imaging tool for patients with suspected LBO. Air-fluid levels can be detected in the dilated colon on erect or supine radiographs [10]. On radiographs, such an air-fluid area can be observed in the upper intestinal tract at the site of obstruction. Air shadows, which are normally seen below the blocked area, are difficult to see. If an obstruction occurs in the upper part of the large intestine, gas is observed in the small intestine, which is not observed in normal cases. The cause of obstruction is more acute when air-fluid levels exist, because the colonic fluid does not remain long enough to be absorbed.

However, the accuracy of plain radiography for the diagnosis of bowel obstruction ranges from 50 to 80%. When the possibility of perforation is considered, an upright chest radiograph or lateral decubitus abdominal film should be obtained to evaluate the pneumoperitoneum [11].

Abdominal radiography can also identify complications of LBO, such as pneumatosis, portal venous gas, and pneumoperitoneum; thus, LBO should be diagnosed with caution. [12,13].

With such limited diagnostic capabilities, further evaluation with multidetector computed tomography (MDCT) may be necessary if such complications or relatively severe conditions are expected [14-16]. However, MDCT is expensive and time consuming, and the radiation exposure is over ten times higher than that of abdominal radiography; thus, it should be used with caution [15].

Another limitation of the diagnostic value of simple, inexpensive abdominal radiography is operator subjectivity. Less experienced pathologists may find it difficult to interpret radiographs of unusual bowel gas patterns [17,18]. To mitigate the subjectivity arising from varying experience, the detection of critical components of related abdominal and intestinal diseases must be automated [9].

From the perspective of radiomics, computerized (semi-) automatic diagnostic procedure for a disease is divided into data acquisition, segmentation, feature extraction, and model evaluation [19,20]. Radiomics includes the computational extraction of the shape, intensity, and appearance descriptors from medical imaging, and when integrated into machine learning algorithms, it can predict outcomes of interest. For LBO diagnosis, several results have been obtained under different conditions [9,21].

However, in the first part of radiomics, that is, data acquisition and segmentation, many parts of the process can be automated with high reliability. Image segmentation is important for disease diagnosis, because it makes digital images easier to analyze. The image is partitioned into multi-

ple nonoverlapping, significantly homogeneous areas during the segmentation process. Segmentation is based on unsupervised clustering techniques, because there is no completely correct ground truth at the pixel level in an image required for supervised learning techniques. Generally, doctors set the suspected area based on a bare-eye investigation with experience, which can cause subjectivity. Automatic segmentation with pixel-level clustering may be a solution to this human error. Developing such system has become challenging in the case of medical imaging owing to poor contrast and noise during acquisition [22, 23], but has shown positive effects in many medical image analysis domains [24-29].

In this study, we propose an automatic segmentation method for identifying air-fluid areas suspicious for LBO from plain erect radiographs. As observed from similar research on detecting suspicious regions with various pixel clustering algorithms [30], erect radiography enables visualizing such areas with image processing and fuzzy clustering algorithms. We also attempted to observe the effect of the Hough transform [31,32] using a traditional edge detection method to locate such regions from the LBO area without a machine learning technique [33]. Based on previous experience, located gas-filled areas from large-bowel images; however, the performance of such an algorithm is weak when the image contains noise. Thus, in this study, we combine a fuzzy unsupervised learning technique to form a robust LBO suspicious region detection method along with a Hough transform that successfully locates the suspicious region.

Among the many fuzzy pixel-clustering algorithms, we selected the fuzzy possibilistic c-means algorithm [34], which has recently shown reliable performance in medical image analysis [35, 36]. Thus, in summary, the method proposed here is a mixture of morphological knowledge of LBO (edge length) in segmentation and fuzzy unsupervised learning at the pixel level to form a robust LBO-suspicious area that can be used to create a reliable set of features for model evaluation in radiomics studies for LBO diagnosis.

II. PROPOSED AUTOMATIC SEGMENTATION METHOD

A. Image Preprocessing

From the input erect radiography, we removed the liver area located above the area of interest and waist and pelvis areas located below our target area using the morphological knowledge that the intestinal region lies within the rib line.

We then applied the Hough transform to locate suspicious LBO regions using Canny edge processing, as shown in [33]. The Hough transform can be defined as the transformation of a point in Cartesian space into a parameter space defined by the shape of the object of interest. We used the technique

explained in [33].

Generally, a medical image analysis algorithm provides auxiliary intensity stretching, that is, a normalization process, to magnify the brightness contrast and effectively differentiate the target object from the background. From the given X-ray image, a similar difficulty arises in adopting fuzzy stretching [25], except that we apply a trapezoid membership function that frequently yields a more stable membership representation. Here, the intensity distribution is irregular compared to that in the usual triangle membership function [37]. This fuzzy stretching method was also used in the preprocessing phase to remove the waist and pelvis areas from the input radiograph in conjunction with Otsu binarization to form a simple LBO-related region-of-interest image. Fig. 1 briefly summarizes the preprocessing effect.

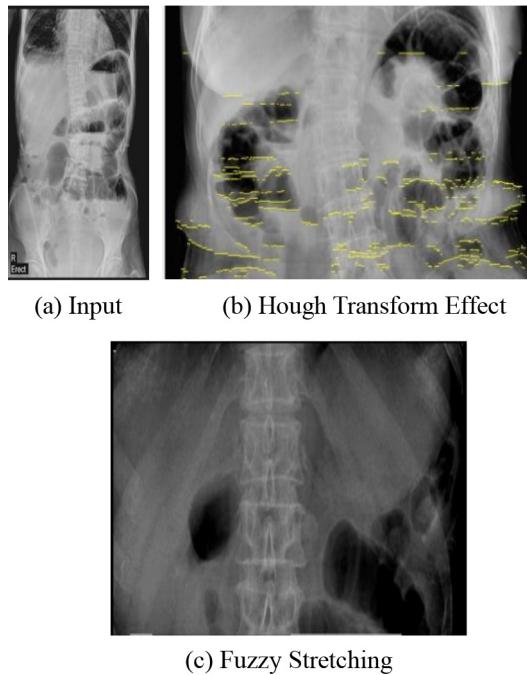


Fig. 1. Effect of Image Preprocessing

B. Possibilistic Fuzzy C-Means Clustering

The most widely used fuzzy clustering algorithm is fuzzy c-means (FCM) [38], which softly classifies images into a predefined number of clusters. FCM clusters are formed with similar data points in the feature space by iteratively minimizing the cost function, which is designed to be proportional to the distance between the pixels and cluster centers in the feature domain. However, FCM has several problems in terms of achieving an optimal solution. One of these drawbacks is that FCM is extremely sensitive to noisy data or outliers. Unfortunately, plain radiography generally con-

tains several types of noise and has low image quality. Thus, FCM must be used with many associated image-processing steps to mitigate the noise effect.

Possibilistic c-means (PCM) [39] was designed to be more robust than FCM in domain applications. The PCM membership degree refers to the degree of ‘typicality’ between data and clusters. PCM relaxes the probabilistic constraint to interpret the membership function or degree of typicality in a possibilistic sense. In our previous study, we found an air-fluid area in the SBO images; however, PCM did not exhibit better performance than FCM [30]. In the previous study, PCM failed since the membership degree of PCM is defined as the degree of ‘typicality’ between data and clusters, which is independent of its relationship to other clusters. The negative effect of this independence is that the PCM may identify overlapping clusters.

Possibilistic fuzzy c-means (PFCM) [34] uses the membership degree of FCM and typicality of PCM to overcome FCM’s noise sensitivity and PCM’s overlapped cluster search problem.

$$J_{PFCM} = \sum_{i=1}^C \sum_{k=1}^N (au_{ik}^m + bt_{ik}^\eta) d_{ik}^2 + \sum_{i=1}^C \delta_i \sum_{k=1}^N (1 - t_{ik})^\eta \tag{1}$$

In Equation (1), a and b are the weight constants for membership and typicality in respectively; η and m are constants representing the same degree of fuzzification satisfying the condition $(m = n) \in (1, \infty)$. d_{ik} is the Euclidean distance between the k-th data point and i-th central vector, as shown in Equation (2).

$$d_{ik} = \|x_{ik} - v_i\| = \left[\sum_{j=1}^p (x_{kj} - v_{ij})^2 \right]^{\frac{1}{2}} \tag{2}$$

where p is the number of dimensions, and the centroid v_i is computed using Equation (3).

$$v_i = \frac{\sum_{k=1}^N (au_{ik}^m + bt_{ik}^\eta) x_k}{\sum_{k=1}^N (au_{ik}^m + bt_{ik}^\eta)} \tag{3}$$

The membership degree u_{ik} and degree of typicality t_{ik} are computed using Equations (4) and (5) as follows:

$$u_{ik} = \left(\sum_{j=1}^c \left(\frac{d_{ik}}{d_{jk}} \right)^{\frac{2}{m-1}} \right)^{-1} \tag{4}$$

$$t_{ik} = \frac{1}{1 + \left(\frac{bd_{ik}^2}{\delta_i} \right)^{\frac{1}{\eta-1}}} \tag{5}$$

In Equation (5), the volume δ_i is computed as

$$\delta_i = K \frac{\sum_{k=1}^n t_{ik}^\eta d_{ik}^2}{\sum_{k=1}^n t_{ik}^\eta} \quad (6)$$

where K is a positive constant and we set $K = 1$.

The flow of the PFCM algorithm applied in this study is illustrated in Fig. 2.

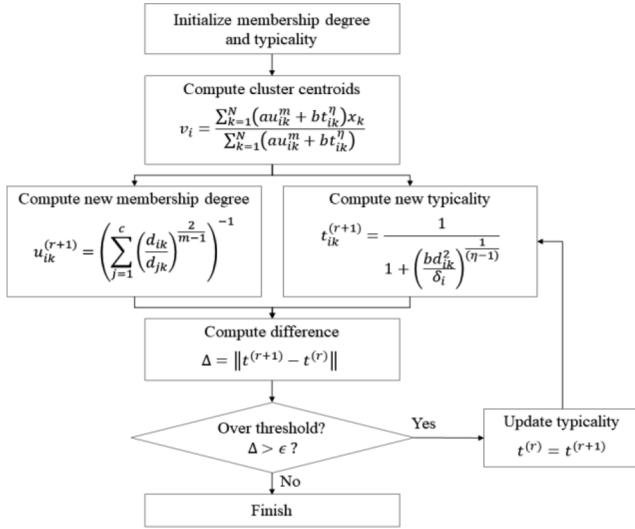


Fig. 2. Flow of the PFCM algorithm

After the PFCM application, we applied the corrosion operation and other image smoothing algorithms to obtain the resultant air-fluid area, as shown in Fig. 3.



Fig. 3. PFCM result

III. RESULTS

The proposed method is implemented using C# under Visual Studio 2019 environment on an IBM PC with Intel(R) Core(TM) i7-8700HQ CPU @ 3.60GHz and 16 GB RAM. In total, 104 X-ray images containing LBO with a size of 1208 × 1502 pixels were used in this experiment. All 104 images were obtained from Gupo Sunsim Hospital, Busan, Korea.

Table 1. Suspicious area extraction rate

| Evaluation | FCM | PCM | PFCM |
|------------|-------|-------|-------|
| Success | 61 | 67 | 73 |
| Partial | 28 | 26 | 21 |
| Fail | 15 | 11 | 10 |
| FullRate | 58.7% | 64.4% | 70.2% |

The performance of the proposed PFCM-based method was compared with that of the FCM- and PCM-based methods, as shown in Table 1, for the LBO suspicious area extraction rate.

Multiple radiologists verified the performance evaluation. In Table 1, ‘success’ indicates that all LBO contained areas were extracted. ‘Partial’ means not all LBO contained area are extracted. The measure ‘fullrate’ means the number of ‘success’ images divided by all 104 input images.

Only the proposed PFCM-based method fully detected the LBO suspicious region per image over 70%; thus, we can conclude that this PFCM, which compensates for FCM and PCM, is feasible for real-world use in suspicious area detection.

We also evaluated all three candidate algorithms to accurately identify suspicious regions at the pixel level. To compute this, we quantified the areas of TP (true positive), FP (false positive), true negatives (TNs), and FN (false negative) for every successfully detected suspicious LBO region. The performance measures were as follows:

$$TPR = \frac{TP}{TP + FN} * 100 \quad (7)$$

$$FPR = \frac{FP}{FP + TN} * 100 \quad (8)$$

$$Precision = \frac{TP}{TP + FP} * 100 \quad (9)$$

$$Accuracy = \frac{TP + TN}{TP + FP + TN + FN} * 100 \quad (10)$$

Again, the proposed PFCM-based method is superior to the FCM and PCM-based methods. Fig. 4 shows the performance of the three algorithms.

Table 2. Pixel level region area detection performance

| Measure | FCM | PCM | PFCM |
|-----------|--------|--------|--------|
| TPR | 76.25% | 79.27% | 91.34% |
| FPR | 3.04% | 3.04% | 2.87% |
| Precision | 91.52% | 90.52% | 96.17% |
| Accuracy | 96.05% | 95.85% | 97.47% |

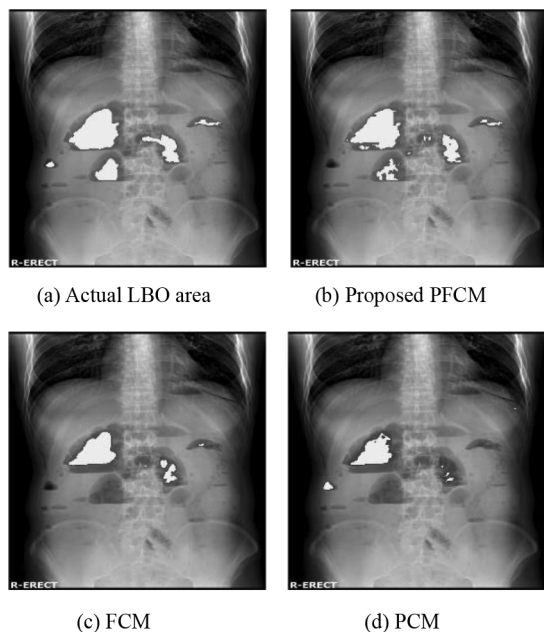


Fig. 4. Visual comparison of three methods

IV. DISCUSSION AND CONCLUSIONS

In this paper, we propose an automatic segmentation method to extract the LBO-suspicious air-fluid area from plain radiographic images. The proposed method combines the Hough transform-based edge-linking method and PFCM pixel clustering method to form the target area from a noisy environment. The Hough transform was used to effectively locate the target area, because the lower part of the intestinal contents formed a straight horizontal line. PFCM is a hybrid unsupervised learning method that combines the cost functions of FCM and PCM to mitigate the drawbacks of noise sensitivity and overlapping cluster searches.

In the experiment with 104 real-world LBO containing radiographs, the proposed PFCM-based method automatically identified the target area fully successfully in 73 images and partially extracted it in another 21 images. This performance is significantly better than those of the PCM- and FCM-based methods. The proposed method, however, failed to find the target area in 10 images because of the extremely low brightness contrast of the input images or because too few clusters were designated in the initialization of PFCM learning. Static initialization of the number of clusters was common to the three clustering strategies used in this experiment.

The proposed method also showed better results than PCM and FCM in pixel-level target object formation. The proposed PFCM-based method demonstrated statistically significant results for all four statistical measures: TPR, FPR, accuracy, and precision.

To improve the performance of the automatic segmentation of LBO, dynamic initialization of the number of clusters for PFCM may be applied. Moreover, a variation of PFCM may be implemented that uses different distance measures in the cluster centroid movement, such as using a Gaussian distribution or other statistical intelligence to guide the search of the target area.

ACKNOWLEDGEMENTS

This manuscript is a partial result of a study on the "Leaders in Industry-university Cooperation 3.0" Project, supported by the Ministry of Education and National Research Foundation of Korea.

REFERENCES

- [1] R. M. Gore, R. I. Silvers, K. H. Thakrar, D. R. Wenzke, U. K. Mehta, G. M. Newmark, and J. W. Berlin, "Bowel obstruction," *Radiologic Clinics*, vol. 53, no. 6, pp. 1225-1240, Nov. 2015. DOI: 10.1016/j.rcl.2015.06.008.
- [2] C.-h. Jeon and C.-s. Cho, "Postoperative adhesive small bowel obstruction treated using acupuncture and moxibustion: A case report," *The Journal of Internal Korean Medicine*, vol. 41, no. 2, pp. 233-240, May 2020. DOI: 10.22246/jikm.2020.41.2.233.
- [3] Healthcare Bigdata Hub. Health insurance review & assessment Service, [Online], Available: <http://opendata.hira.or.kr/op/opc/olap3thDsInfo.do>.
- [4] F. Catena, B. De Simone, F. Coccolini, S. Di Saverio, M. Sartelli, and L. Ansaloni, "Bowel obstruction: a narrative review for all physicians," *World Journal of Emergency Surgery*, vol. 14, no. 1, pp. 1-8, Apr. 2019. DOI: 10.1186/s13017-019-0240-7.
- [5] S. M. Bahouth, "Mechanical Obstruction: Large Bowel Obstruction (LBO)," in *Essential Radiology Review, Springer, Cham*, pp. 289-290. 2019. DOI: 10.1007/978-3-030-26044-6_86.
- [6] R. Frago, E. Ramirez, M. Millan, E. Kreisler, E. del Valle, and S. Biondo, "Current management of acute malignant large bowel obstruction: a systematic review," *The American Journal of Surgery*, vol. 207, no. 1, pp. 127-138, Jan. 2014. DOI: 10.1016/j.amjsurg.2013.07.027.
- [7] A. K. Pujahari, "Decision making in bowel obstruction: a review," *Journal of clinical and diagnostic research: Journal of Clinical and Diagnostic Research*, vol. 10, no. 12, pp. PE07-PE12, Dec. 2016. DOI: 10.7860/JCDR/2016/22170.8923.
- [8] P. Taourel, N. Kessler, A. Lesnik, J. Pujol, L. Morcos, and J.-M. Bruel, "Helical CT of large bowel obstruction," *Abdom Imaging*, vol. 28, no. 2, pp. 267-275, Mar. 2003. DOI: 10.1007/s00261-002-0038-y.
- [9] Y. Tamyalew, A. O. Salau, and A. M. Ayalew, "Detection and classification of large bowel obstruction from X-ray images using machine learning algorithms," *International Journal of Imaging Systems and Technology*, vol. 33, no. 1, pp. 158-174, Sep. 2022. DOI: 10.1002/ima.22800.
- [10] R. M. Gore and M. S. Levine, *Textbook of gastrointestinal radiology*. 3rd ed. Philadelphia, PA: Saunders/Elsevier, 2008.
- [11] D. W. Nelms and B. R. Kann, "Imaging modalities for evaluation of intestinal obstruction," *Clinics in colon and rectal surgery*, vol. 34, no. 4, pp. 205-218, Jun. 2021. DOI: 10.1055/s-0041-1729737.

- [12] R. E. Kottler and G. K. Lee, "The threatened caecum in acute large-bowel obstruction," *The British Journal of Radiology*, vol. 57, no. 683, pp. 989-990, Nov. 1984. DOI: 10.1259/0007-1285-57-683-989.
- [13] P. Taourel, F. Garibaldi, J. Arrigoni, V. Le Guen, A. Lesnik, and J.-M. Bruel, "Cecal pneumatosis in patients with obstructive colon cancer: correlation of CT findings with bowel viability," *American Journal of Roentgenology*, vol. 183, no. 6, pp. 1667-1671, Dec. 2004. DOI: 10.2214/ajr.183.6.01831667.
- [14] L. Plastaras, L. Vuitton, N. Badet, S. Koch, V. Di Martino, and E. Delabrousse, "Acute colitis: Differential diagnosis using multidetector CT," *Clinical Radiology*, vol. 70, no. 3, pp. 262-269, Mar. 2015. DOI: 10.1016/j.crad.2014.11.008.
- [15] C. Duffin, S. Mirpour, T. Catanzano, and C. Moore, "Radiologic imaging of bowel infections," *Seminars in Ultrasound, CT and MRI*, WB Saunders, vol. 41, no. 1, pp. 33-45, Feb. 2020. DOI: 10.1053/j.sult.2019.10.004.
- [16] J. D. Patel, H. I. Gale, and K. J. Chang, "Imaging of large bowel with multidetector row CT," in *Multislice CT*, Springer, Cham, pp. 641-665, Feb. 2017. DOI: 10.1007/174_2017_7.
- [17] C. J. Das, S. Manchanda, A. Panda, A. Sharma, and A. K. Gupta, "Recent advances in imaging of small and large bowel," *PET clinics*, vol. 11, no. 1, pp. 21-37, Jan. 2016. DOI: 10.1016/j.cpet.2015.07.008.
- [18] W. Z. Geng, M. Fuller, B. Osborne, and K. Thoirs, "The value of the erect abdominal radiograph for the diagnosis of mechanical bowel obstruction and paralytic ileus in adults presenting with acute abdominal pain," *Journal of Medical Radiation Sciences*, vol. 65, no. 4, pp. 259-266, Jul. 2018. DOI: 10.1002/jmrs.299.
- [19] J. M. Miranda Magalhaes Santos, B. Clemente Oliveira, J. D. A. B. Araujo-Filho, A. N. Assuncao-Jr, F. A. de M. Machado, C. Carlos Tavares Rocha, J. V. Horvat, M. R. Menezes, and N. Horvat, "State-of-the-art in radiomics of hepatocellular carcinoma: a review of basic principles, applications, and limitations," *Abdominal Radiology*, vol. 45, no. 2, pp. 342-353, Nov. 2019. DOI: 10.1007/s00261-019-02299-3.
- [20] A. S. Alyami, "The Role of Radiomics in Fibrosis Crohn's Disease: A Review," *Diagnostics*, vol. 13, no. 9, p. 1623, May 2023. DOI: 10.3390/diagnostics13091623.
- [21] S. Park, J. C. Ye, E. S. Lee, G. Cho, J. W. Yoon, J. H. Choi, I. Joo, and Y. J. Lee, "Deep learning-enabled detection of pneumoperitoneum in supine and erect abdominal radiography: Modeling Using Transfer Learning and Semi-Supervised Learning," *Korean Journal of Radiology*, vol. 24, no. 6, pp. 541-552, Jun. 2023. DOI: 10.3348/kjr.2022.1032.
- [22] W. Bo, W. ying, and C. Lijie, "Fuzzy clustering recognition algorithm of medical image with multi-resolution feature," *Concurrency and Computation: Practice and Experience*, vol. 32, no. 1, p. e4886, Jan. 2020. DOI: 10.1002/cpe.4886.
- [23] K. Xia, X. Gu, and Y. Zhang, "Oriented grouping-constrained spectral clustering for medical imaging segmentation," *Multimedia Systems*, vol. 26, pp. 27-36, Feb. 2020. DOI: 10.1007/s00530-019-00626-8.
- [24] J. Park, D. H. Song, H. Nho, H. Choi, K. A. Kim, H. J. Park, and K. B. Kim, "Automatic segmentation of brachial artery based on fuzzy C-means pixel clustering from ultrasound images," *International Journal of Electrical and Computer Engineering*, vol. 8, no. 2, pp. 638-643, Apr. 2018. DOI: 10.11591/ijece.v8i2.pp638-643.
- [25] K. B. Kim, D. H. Song, and S. S. Yun, "Automatic segmentation of wrist bone fracture area by K-means pixel clustering from X-ray image," *International Journal of Electrical and Computer Engineering*, vol. 9, no. 6, pp. 5205-5210, Dec. 2019. DOI: 10.11591/ijece.v9i6.pp5205-5210.
- [26] F. Cervantes-Sanchez, I. Cruz-Aceves, A. Hernandez-Aguirre, M. A. Hernandez-Gonzalez, and S. E. Solorio-Meza, "Automatic segmentation of coronary arteries in X-ray angiograms using multiscale analysis and artificial neural networks," *Applied Sciences*, vol. 9, no. 24, p. 5507, Dec. 2019. DOI: 10.3390/app9245507.
- [27] K. B. Kim, G. H. Kim, D. H. Song, H. J. Park, and C. W. Kim, "Automatic segmentation of liver/kidney area with double-layered fuzzy C-means and the utility of hepatorenal index for fatty liver severity classification," *Journal of Intelligent & Fuzzy Systems*, vol. 39, no. 1, pp. 925-936, Jul. 2020. DOI: 10.3233/JIFS-191850.
- [28] W. Shen, W. Xu, H. Zhang, Z. Sun, J. Ma, X. Ma, et al., "Automatic segmentation of the femur and tibia bones from X-ray images based on pure dilated residual U-Net," *Inverse Problems and Imaging*, vol. 15, no. 6, pp. 1333-1346, Dec. 2021. DOI: 10.3934/ipi.2020057.
- [29] K. B. Kim, D. H. Song, and H. J. Park, "Robust Automatic Segmentation of Inflamed Appendix from Ultrasonography with Double-Layered Outlier Rejection Fuzzy C-Means Clustering," *Applied Sciences*, vol. 12, no. 11, p. 5753, Jun. 2022. DOI: 10.3390/app12115753.
- [30] K. B. Kim, "Performance evaluation of pixel clustering approaches for automatic detection of small bowel obstruction from abdominal radiographs," *Journal of information and communication convergence engineering*, vol. 20, no. 3, pp. 153-159, Sep. 2022. DOI: 10.56977/jicce.2022.20.3.153.
- [31] R. O. Duda and P. E. Hart, "Use of the Hough transformation to detect lines and curves in pictures," *Communication of Association for Computing Machinery (ACM)*, vol. 15, no. 1, pp. 11-15, Jan. 1972. DOI: 10.1145/361237.361242.
- [32] H. M. Ünver, Y. Kökver, E. Duman, and O. A. Erdem, "Statistical edge detection and circular hough transform for optic disk localization," *Applied Sciences*, vol. 9, no. 2, p. 350, Jan. 2019. DOI: 10.3390/app9020350.
- [33] K. B. Kim, D. H. Song, and Y. W. Woo, "Automatic segmentation of large bowel obstruction area with Hough transform from erect abdominal radiograph images," *International Journal of Electrical and Computer Engineering*, vol. 11, no. 3, pp. 2674-2649, Jun. 2021. DOI: 10.11591/ijece.v11i3.pp2674-2679.
- [34] N. R. Pal, K. Pal, J. M. Keller, and J. C. Bezdek, "A possibilistic fuzzy c-means clustering algorithm," *IEEE Transactions on Fuzzy System*, vol. 13, no. 4, pp. 517-530, Aug. 2005. DOI: 10.1109/TFUZZ.2004.840099.
- [35] M. H. F. Zarendi, S. Sotudian, and O. Castillo, "A new validity index for fuzzy-possibilistic c-means clustering," *arXiv preprint arXiv: 2005.09162*, May 2020. DOI: 10.48550/arXiv.2005.09162.
- [36] C. L. Chowdhary and D. P. Acharjya, "Clustering algorithm in possibilistic exponential fuzzy C-mean segmenting medical images," in *Journal of Biomimetics, biomaterials and biomedical engineering*, vol. 30, pp. 12-23, Jan. 2017. DOI: 10.4028/www.scientific.net/JBBBE.30.12.
- [37] K. B. Kim and D. H. Song, "Intelligent automatic extraction of canine cataract object with dynamic controlled fuzzy C-means based quantization," *International Journal of Electrical and Computer Engineering*, vol. 8, no. 2, pp. 666-672, Apr. 2018. DOI: 10.11591/ijece.v8i2.pp666-672.
- [38] R. Suganya and R. Shanthi, "Fuzzy c-means algorithm-a review," *International Journal of Scientific and Research Publications*, vol. 2, no. 11, pp. 440-442, Nov. 2012.
- [39] R. Krishnapuram and J. M. Keller, "A possibilistic approach to clustering," *IEEE Transactions on Fuzzy Systems*, vol. 1, no. 2, pp. 98-110, May 1993. DOI: 10.1109/91.227387.



Kwang Baek Kim

Kwang Baek Kim received his M.S. and Ph.D. degrees from the Department of Computer Science, Pusan National University, Busan, Korea in 1993 and 1999, respectively. From 1997–2020, he was a professor at the Department of Computer Engineering, Silla University, Korea. From 2021 to the present, he is a professor at the Department of Artificial Intelligence, Silla University, Korea. He is currently an associate editor for Journal of Intelligence and Information Systems. His research interests include fuzzy clustering and applications, machine learning, and image processing.



Emeritus Professor Doo Heon Song

received his B.S. from Seoul National University and M.S. from the Korea Advanced Institute of Science and Technology in Computer Science. He received his Ph.D. candidate Certificate in Computer Science from the University of California at Irvine in 1994. He has been a professor at Department of Computer Games, Yong-in Art & Science University in Korea since 1997 and currently holds the Emeritus professor title. He has published over 130 research papers in SCIE/SCOPUS/KCI journals and another 130 domestic/international conference papers in areas of machine learning, fuzzy systems, medical image analysis, and computer game design.



Hyun Jun Park

Hyun Jun Park received his M.S. and Ph.D. degrees from the Department of Computer Engineering, Pusan National University, Busan, Korea, in 2009 and 2017, respectively. In 2017, he was a postdoctoral researcher at BK21PLUS, Creative Human Resource Development Program for IT Convergence, Pusan National University, Korea. From 2018 to the present, he has worked as an assistant professor at the Department of Artificial Intelligence Software, Cheongju University, Korea. His research interests include computer vision, image processing, factory automation, neural network, and deep learning applications.